Thermospheric Density Perturbations Produced by Traveling Atmospheric Disturbances during August 2005 Storm

K. H. Pham[1], B. Zhang[1,2], K. Sorathia[3], T. Dang[4], W. Wang[1], V. Merkin[3], Huixin Liu[5], D. Lin[1], M. Wiltberger[1], J. Lei[4], S. Bao[6], J. Garretson[3], F. Toffoletto[6], A. Michael[3], J. Lyon[7]

[1] High Altitude Observatory, National Center for Atmospheric Research, Boulder, Colorado, USA.

[2] Department of Earth Sciences, University of Hong Kong, Pokfulam, Hong Kong.

[3] Applied Physics Laboratory, Johns Hopkins University, Laurel, Maryland, USA.

[4] CAS Key Laboratory of Geospace Environment, School of Earth and Space Sciences, University of Science and Technology of China, Hefei, China

[5] Department of Earth and Planetary Science, Kyushu University, Fukuoka, Japan

[6] Department of Physics and Astronomy, Rice University, Houston TX

[7] Thayer School of Engineering, Dartmouth College, Hanover, New Hampshire, USA.

Corresponding author: Kevin Pham (phamkh@ucar.edu)

Key Points:

- Most neutral density peaks observed by CHAMP and GRACE during a geomagnetic storm are associated with traveling atmospheric disturbances
- TADs generated at high-latitudes propagate globally and interfere to produce large amplitude enhancements at lower latitudes
- A coupled geospace model with high spatial resolving power is necessary to properly resolve TADs observed by CHAMP and GRACE

Abstract

Thermospheric mass density perturbations are commonly observed during geomagnetic storms. The sources of these perturbations have not been well understood. In this study, we investigated the thermospheric density perturbations observed by the CHAMP and GRACE satellites during the 24-25 August 2005 geomagnetic storm. The observations show that large neutral density enhancements occurred not only at high latitudes, but also globally. In particular, large density perturbations were seen in the equatorial regions away from the high-latitude, magnetospheric energy sources. We used the high-resolution Multiscale Atmosphere Geospace Environment (MAGE) model to reproduce the consecutive neutral density changes observed by the satellites during the storm. The MAGE simulation, which resolved mesoscale high-latitude convection electric fields and field-aligned currents, and included a physics-based specification of the auroral precipitation, was contrasted with a standalone ionosphere-thermosphere simulation driven by an empirical model of the high-latitude electrodynamics. The comparison demonstrates that a first-principles representation of highly dynamic and localized Joule heating events in a fully coupled whole geospace model such as MAGE is critical to accurately capturing both the generation and propagation of traveling atmospheric disturbances (TADs) that produce neutral density perturbations globally. In particular, the MAGE simulation shows that the larger density peaks in the equatorial region that are observed by CHAMP and GRACE are the results of TADs, generated at high latitudes in both hemispheres, propagating to and interfering at lower latitudes. This study reveals the importance of investigating thermospheric density variations in a fully coupled geospace model with sufficiently high resolving power.

Plain Language Summary

During geomagnetic storms, increased activity within the geospace environment causes large scale plasma convection to occur and electrons to precipitate into the upper atmosphere. The enhanced heating of the thermosphere by the plasma convection and electron precipitation can produce large perturbations in the neutral density. These neutral density perturbations propagate away from their point of origin, oftentimes traveling to the equator and into the other hemisphere. Simulation results using a high resolution coupled geospace model that includes a magnetosphere, inner magnetosphere, ionosphere, and thermosphere model show that neutral density perturbations generated in one hemisphere can propagate far enough to interfere with those in the other hemisphere. The interference of two or more perturbations produces a region of larger neutral density perturbations. The high resolution coupled geospace model performs significantly better than the standalone model when compared to observations of neutral density by low altitude spacecraft. A significant fraction of the observed neutral density perturbations are captured by the coupled model, especially those are lower latitudes.

1 Introduction

Thermospheric mass density enhancements observed by the Challenging Minisatellite Payload (CHAMP) and the Gravity Recovery and Climate Experiment (GRACE) satellites in the polar cap are well known to be primarily magnetospheric origin. The background neutral density is controlled by solar irradiance while magnetospheric interactions with the solar wind can transport energy along field lines into the ionosphere-thermosphere where they cause neutral density and composition perturbations (Prölss, 2011). During geomagnetic storms, Liu et al. (2010) detected neutral density enhancement events in the polar cap of 90% of the 29 storms with Dst < -100nT

that were examined, indicating that neutral density enhancements in the polar cap are not rare. Understanding the source of and magnetospheric impact on the density enhancements is crucial to the magnetosphere-ionosphere-thermosphere (MIT) coupling physics, and has been a long-standing issue.

Prior studies have examined the neutral density enhancements and the associated Joule heating imposed by magnetospheric energy input. Electromagnetic energy dissipated as Joule heating in the upper atmosphere is related to the amount of downward Poynting flux, especially in regions of high conductance (Kelley et al., 1991; Richmond 2010; Vanhamki, et c., 2012). However, the spatial distribution of large-scale density enhancements does not correlate well with the distribution of Poynting flux (Billett et al., 2021) and nearly 50% of polar cap density enhancements events do not have concurrent increases in energy input as seen in field-aligned-current (FAC) structures (Liu et al., 2010). Bruinsma and Forbes (2007, 2009) and Lu et al. (2016) found that polar cap mass density enhancements could arise from passage of traveling atmospheric disturbances (TADs) that have propagated across the polar cap and subsequently toward the equator, suggesting that direct energy inputs at the density enhancement location is not required. In fact, density and temperature enhancements have been found to not occur right at the location of the strongest Joule heating, but rather regions of strong downwelling of the air (Burns et al., 1995; Wang et al., 2012). Heating of the thermosphere can produce TADs, which are associated with transient neutral density structures (e.g., Forbes et al., 2005; Bruinsma and Forbes, 2010) that perturb the background neutral density as TADs propagate equatorward with speeds near the local sound speed and are also frequently observed in the mid- and low- latitudes (Mayr et al., 1990; Bruinsma and Forbes, 2009, and references therein).

The source, properties, and evolution of neutral density perturbations and TADs are not easily addressed with limited in-situ observations (Bruinsma and Forbes, 2009). Extensive modeling work has been performed to improve the description of storm-time thermospheric heating resulting from the interaction with the magnetosphere, including improved empirical specifications (Weimer, 2005), data assimilation models (Lu et al., 2016), or coupling to physics-based magnetosphere models (e.g., Connor et al., 2016; Wang et al., 2004). Other attempts to reproduce neutral density perturbations have added additional physics to coupled MIT models such as soft precipitation (Zhang et al., 2012; Deng et al., 2013), and Alfven wave heating (Hogan et al., 2020). These have all demonstrated some success in capturing statistical properties (Zhang et al, 2012; Deng et al., 2013) or longer duration orbit averages (Lei et al., 2010; Hogan et al., 2020) of neutral density enhancements observed by CHAMP. While coupled models produce neutral density enhancements more self-consistently, the transient nature and timescale of TADs and associated perturbations require sufficient model resolution and an accurate representation of the relevant physical processes to resolve the localized generation and propagation of TADs. Therefore, a detailed comparison with the data and successful capture of the density structures along each satellite orbit has not been achieved by simulations to our best knowledge. Increased resolution is necessary in the magnetosphere-ionosphere models to improve the structure of high-latitude FAC (Honkonen et al., 2013; Wiltberger et al., 2017) to better represent the location and strength of Joule heating and thus the generation of TADs. High resolution thermosphere-ionosphere models also can better represent mesoscale structures of Joule heating (Matsuo and Richmond, 2008) and improve their capability to resolve the propagation of TADs and their associated density structures (Dang et al., 2018). Therefore, a coupled MIT model capable of properly capturing the generation,

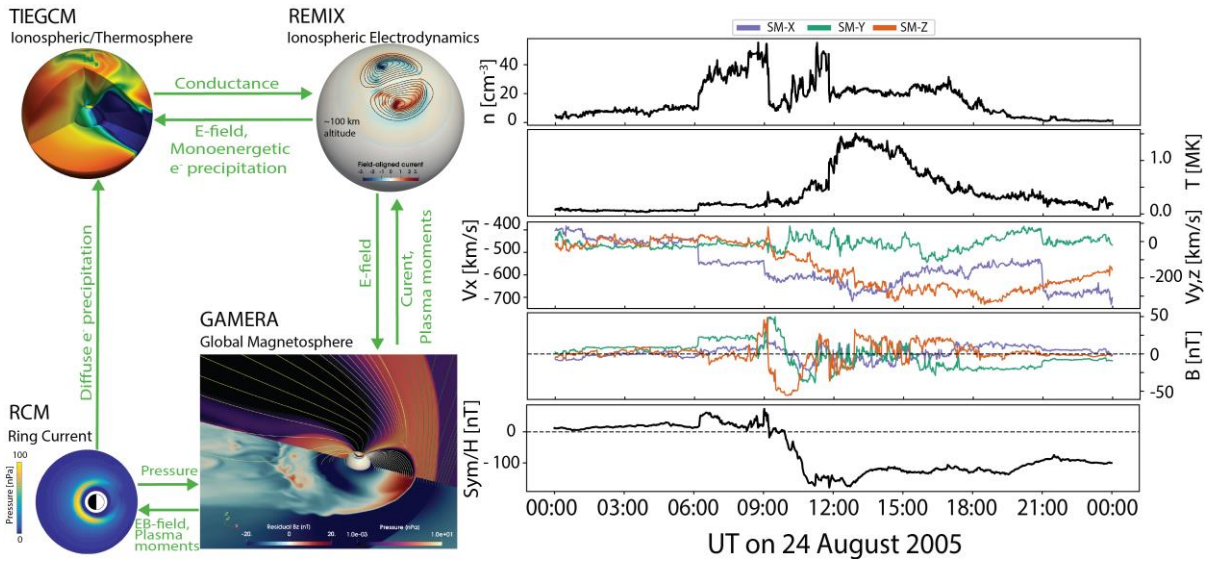

Figure 1: The MAGE coupling scheme (left) depicting the coupling procedure and variables that are passed between models. The solar wind, and interplanetary magnetic field conditions and SYMH (right) for 24 August 2005.

resolution, and transport of TADs is critical to understanding thermospheric neutral density enhancements produced by TADs.

Using a coupled geospace model with high spatial resolving power, we demonstrate that a significant number of density enhancements seen by satellites along satellite orbits at all latitudes during a single storm on 24 August 2005 are actually TADs that were generated at high-latitudes. The Multiscale Atmosphere Geospace Environment (MAGE) model used in this study couples multiple first-principles, high-resolution models of different geospace domains together into a cohesive geospace model and represents a significant advancement in modeling the geospace environment. We also demonstrate that a coupled geospace model with high-resolution is critical in simulating the TAD properties and ultimately, whether the neutral density enhancements as measured by CHAMP and GRACE are captured by the model.

2 Model Description

This study uses the current iteration of the MAGE model which two-way couples the Grid Agnostic MHD Environment for Research Applications (GAMERA) global magnetospheric MHD model (Zhang et al., 2019a; Sorathia et al., 2020), the Rice Convection Model (RCM) (Toffoletto et al., 2003), the Thermosphere-Ionosphere Electrodynamic General Circulation Model (TIEGCM) (Richmond et al., 1992; Qian et al., 2014), and the RE-developed Magnetosphere-Ionosphere Coupler/Solver (REMIX), which is a rewrite of the MIX code (Merkin and Lyon, 2010). A schematic of how the components of the MAGE model are coupled together and the input solar wind/interplanetary magnetic field conditions for both the MAGE model and the WEIMER empirical high-latitude convection model (Weimer, 2015) that is used to drive the standalone TIEGCM for the 2005 August 24 event can be found in Figure 1a.

The CHAMP and GRACE observations of the 2005 August 24 geomagnetic storm have been previously studied at length (e.g., Crowley Krauss et al., 2015; Oliveira and Zesta, 2019). Crowley

et al. (2010) simulated 3 CHAMP orbits near the start of the storm using AMIE as the high latitude driver and saw some improvement in capturing density enhancements near the cusp. However, their simulation struggled to capture the amplitude of the enhancement and variability. Krauss et al. (2018) found that while the CHAMP and GRACE spacecraft are at similar altitudes, the amount of orbital decay experienced during this storm is extremely different, with CHAMP experiencing up to 3 times larger orbital decay than GRACE. The large difference in orbital decay throughout this event presents a challenge to global models to capture the characteristics seen by both satellites simultaneously.

GAMERA solves the single fluid magnetohydrodynamic equations using a 7^{th}-order reconstruction scheme on a nonorthogonal-structured grid that has 192, 192, and 256 cells in the radial, meridional and azimuthal directions, respectively. This maps approximately 600km resolution in the plasmasheet. The grid places higher resolution in important magnetospheric regions such as the bow shock, magnetopause, plasmasheet, and near the low-altitude (inner) boundary. The combination of a high order reconstruction scheme with aggressive flux limiting is key to properly resolving the generation and transport of structures with a minimal number of cells (Zhang et al., 2019a).

At the inner boundary of GAMERA, the grid maps to approximately 0.5° in the polar ionosphere which is also the chosen resolution for the REMIX grid. REMIX solves Poisson's equation to obtain the electrostatic potential. The monoenergetic precipitation is calculated from MHD parameters following the Zhang et al. (2015) formulation. To represent the diffuse precipitation, we integrate the electron channels in RCM to obtain the electron flux in the loss cone, thus improving upon the MHD specification of Zhang et al. (2015) by including the RCM drift physics. The REMIX grid is 0.5° in latitude and longitude with low-latitude boundary at 45° magnetic latitude. This translates to 90 and 720 cells in the latitudinal and longitudinal directions, respectively. RCM solves the bounce-averaged drift motion of ions and electrons in the inner magnetosphere with 180 and 361 cells in latitudinal and longitudinal directions and 115 energy channels each for ions and electrons. TIEGCM solves for the chemistry and dynamics of both neutrals and ions in the upper atmosphere ranging from 97km up to approximately 500km at solar min and 700km at solar max. The high-resolution TIEGCM applies ring-average filtering (Zhang et al., 2019b) to increase the resolution a globally uniform 0.625° in both latitudinal and longitudinal directions (Dang et al., 2021). The vertical resolution of the TIEGCM is a quarter of a scale height. This translates to 288, 576, and 57 cells in latitude, longitude, and altitude, respectively.

Typically, when not coupled to a magnetospheric model, high-latitude convection in TIEGCM is specified by either Weimer (Weimer, 2005) or Heelis (Heelis et al., 1982) empirical models. For this study, the neutral densities from the standalone TIEGCM driven by the widely used Weimer empirical model is contrasted with MAGE results to provide a clear example of improvements enabled by a comprehensive geospace coupled model. The Weimer model is widely used as the empirical specification for the high latitude convection of choice for most of the thermosphere-ionosphere models within the community (Krall et al., 2014; Fok et al., 2014; Guo et al., 2019), including the standalone TIEGCM (Qian et al., 2014). In addition, the electron precipitation calculated based on MHD parameters in MAGE are also significantly more self-consistent and dynamic than those specified in the standalone TIEGCM (Roble and Ridley, 1987). We denote

the run where the standalone TIEGCM was driven by the Weimer model to be simply the WEIMER run.

While the storm occurred on 2005 August 24, the model runs started on 2005 August 23 at 12 UT to provide ample time to precondition the models properly. Because 2005 August 23 has relatively quiet conditions, we opted to only show results for 2005 August 24. During this event, both CHAMP and GRACE spacecraft were present and together, cover two different local times (LT). The neutral densities derived from CHAMP and GRACE (Sutton, 2011) were mapped to 400km altitude by assuming diffusive equilibrium at a constant temperature using the MSIS model. The MAGE and WEIMER results extracted at the CHAMP and GRACE positions at 400km altitude are compared to the derived neutral densities.

3 Results

The cross polar cap potential (CPCP) for the northern (Figure 2a) and southern (Figure 2b) hemispheres from MAGE is significantly dynamic, consistent with the changes in solar wind conditions shown in Figure 1. Similarly, the MAGE simulated hemispherically integrated Joule heating (JH, Figure 2c and 2d) also shows strong temporal variations. For comparison, the CPCP and Joule heating in the standalone TIEGCM driven by the Weimer model are also shown in Figure 1. The temporal trends of these two parameters from the two model outputs are similar, which is not surprising as they correlate with the solar wind driving. The CPCP from MAGE is persistently higher than WEIMER's CPCP, consistent with prior works using MHD models of the magnetosphere (e.g., Connor et al., 2016; Wiltberger et al., 2017; Mukhopadhyay et al., 2021). Other data-based methods such as AMIE and SuperDARN also persistently underestimate the CPCP as measured by DMSP (Kihn et al., 2006; Xu et al., 2008). Additionally, while the difference

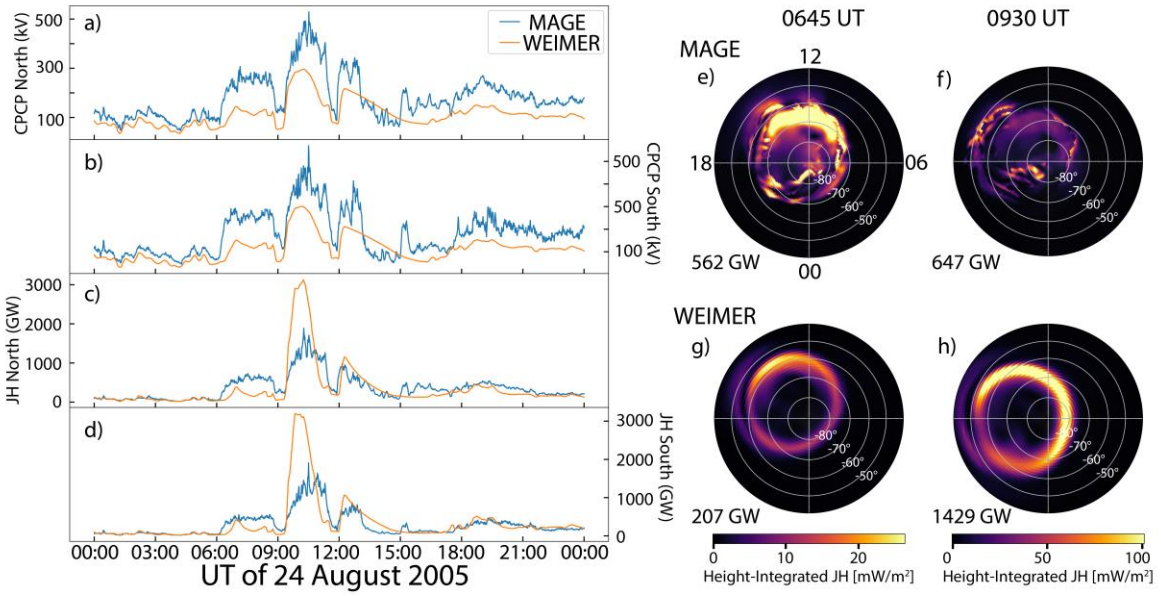

Figure 2: The cross polar cap potential (CPCP) for the northern (a), and southern hemisphere (b) for MAGE and WEIMER runs. The hemispherically integrated Joule heating for northern (c) and southern hemisphere (d) are also included. The panels are height-integrated Joule heating rates for MAGE (top) and WEIMER (bottom) during the early active period at 0645 UT (left) and near peak of the storm at 09:30 UT (right).

in CPCP is larger during active periods, the resulting JH into the ionosphere-thermosphere in the coupled MAGE was actually lower than WEIMER. The difference between JH and CPCP trends is most likely a result of differing electric fields between the models and the underlying conductance distributions. This reflects the complexity and intertwined nature of the coupled system and the need for a coupled model to better capture the intricacies of the MIT coupling. This also indicates that global parameters such as CPCP may not fully capture the localized and dynamic nature of the regional mesoscale structures of Joule heating, which is determined by the strength of electric fields and the ionospheric conductivity strongly regulated by particle precipitation at a particular location. This is further illustrated in the right-hand side top panels in Figure 2, which show the JH distribution calculated by MAGE during the early main phase (07 UT) and late main phase (10 UT) during the storm event. We note above that the JH distribution and structure includes contributions from electron precipitation by enhancing ionospheric ionization and conductivity, with the auroral arc associated with diffuse electron precipitation appearing prominently in MAGE results. During the early main phase, MAGE Joule heating distribution contained many localized heating zones which contributes to a large hemispherically integrated power of 472 GW. During the later main phase, the MAGEMAGE JH behaved similarly with significantly finer detail and mainly localized heating regions. Note that the color scales are different for these two subplots. The hemispherically integrated Joule heating rate at this time is 1266 GW. The bottom panels show the Joule heating patterns from the Weimer run which were much smoother with large broad structures due to its empirical and statistical nature, with a total JH of 382 GW and 2910 GW at two UTs, respectively. Note that Weimer JH was smaller than that in MAGE in the early main phase, but is over a factor of two larger in the later phase. This difference is significant for locations and amplitudes of storm-time TADs that are generated at high-latitude by thermospheric temperature changes associated with Joule heating as shown below.

A comparison of the 1-minute modeled neutral density at 400km with the observation derived density data along the CHAMP and GRACE tracks is given in Figure 3 for both MAGE and WEIMER (Figure 3) runs. MAGE is able to capture both the variability and magnitude of the most of the neutral density enhancements. To better quantitatively describe the data-model performance, we split the event into three parts as shaded in Figure 3: the quiet conditions (yellow), the storm main phase (blue), and the recovery phase (green). The quiet period is defined as everything before the sudden storm commencement (SSC) at 6 UT. In this period, CHAMP and GRACE observed less and very minor enhancements in the neutral densities; we consider everything after the SSC is part of the storm main phase until the DST trends upwards at 13:00 UT; and the recovery phase is everything afterwards until the end of the day. Table 1 summarizes how well the models (MAGE and Weimer) perform compared with the CHAMP and GRACE observations.

During the quiet period, there are no large density enhancements along the tracks, and it is difficult to identify any discernable differences between the models. Earlier in the main phase, MAGE captures density enhancements near 07:30, 08:20, and 09:00 UT, which WEIMER almost all misses. During the most active period, WEIMER performs poorly by both overestimating the observed enhancements and also generating enhancements that are not observed, while MAGE captures a significant fraction of the observed enhancements. The recovery phase exhibits a similar trend, with WEIMER performing especially poor between 15:00 UT through 18:00 UT. Overall, MAGE matches the morphology of neutral density and magnitude of the enhancements observed by CHAMP and GRACE significantly better than WEIMER.

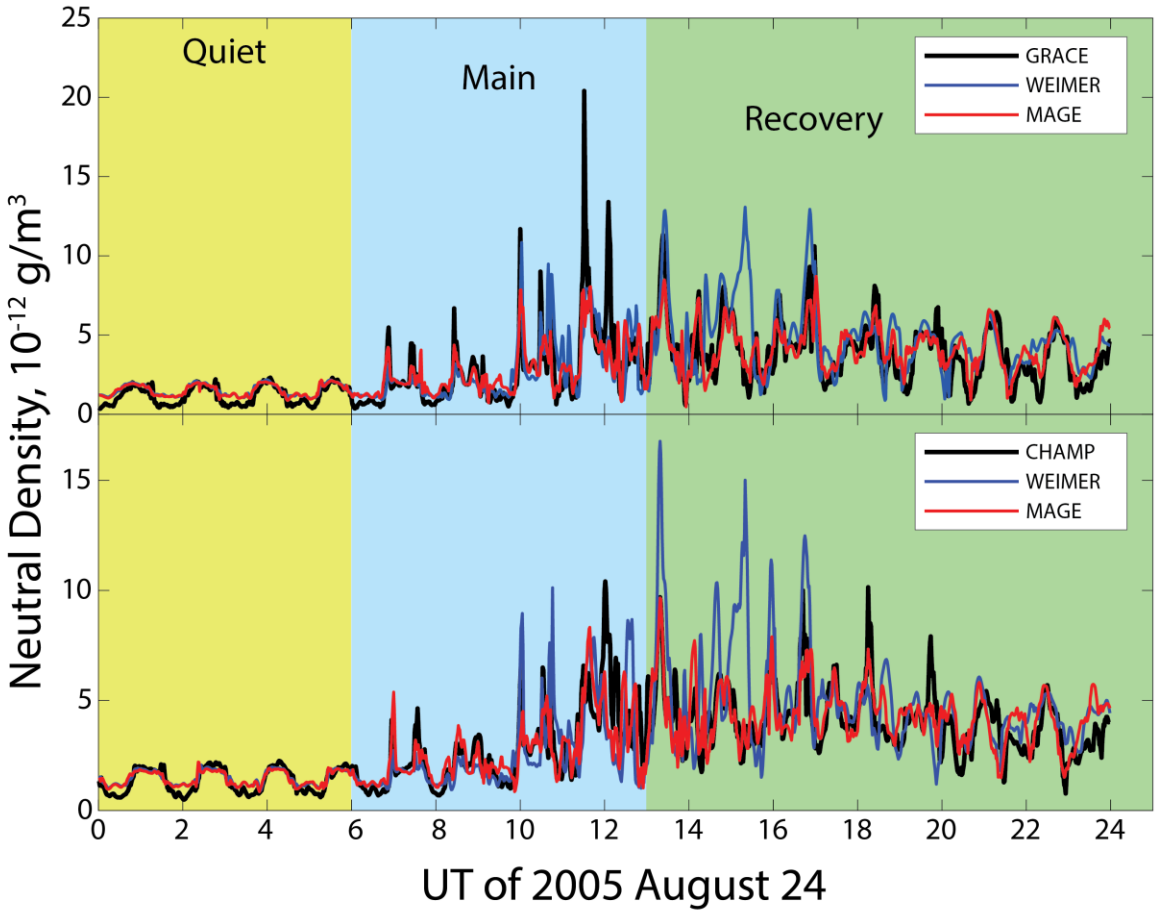

Figure 3: Modeled neutral density along the GRACE (top) and CHAMP (bottom) trajectory from the WEIMER (blue) and MAGE (red) simulations. The shaded regions correspond to the quiet (yellow), main (blue), and recovery (green) phases.

Note here that TIEGCM is the I-T model with 0.625^0 resolution that is used for both MAGE and Weimer runs. The difference between the two runs is that MAGE uses convection pattern and precipitation that is self-consistently calculated within a fully coupled whole geospace model, including the interaction between solar wind and the magnetosphere, magnetosphere dynamics, ring current and precipitation, and their electrodynamic coupling with the I-T, whereas high latitude inputs in Weimer run are empirically specified. This demonstrates the importance of having not only high resolution, but also an accurate physics description of the MIT coupling to capture the storm-time temporospatial variability in the I-T system with high fidelity. This point is further illustrated in Figure 4.

While agreement with observed neutral densities during the quiet and late recovery phases can be easily seen in Figure 3, agreement and details of where disagreements occur are difficult to ascertain from Figure 3. Examining a shorter period spanning 09:00 UT and 17:00 UT, and with the orbital latitude (Figure 4) reveals that WEIMER tends to generate neutral density perturbations in the northern high latitude, when none are observed, for instance at 15:15 UTUT for both CHAMP and GRACE data, and it also overestimates the perturbations seen in the southern hemisphere. On the other hand, MAGE captures CHAMP and GRACE reasonably well at all

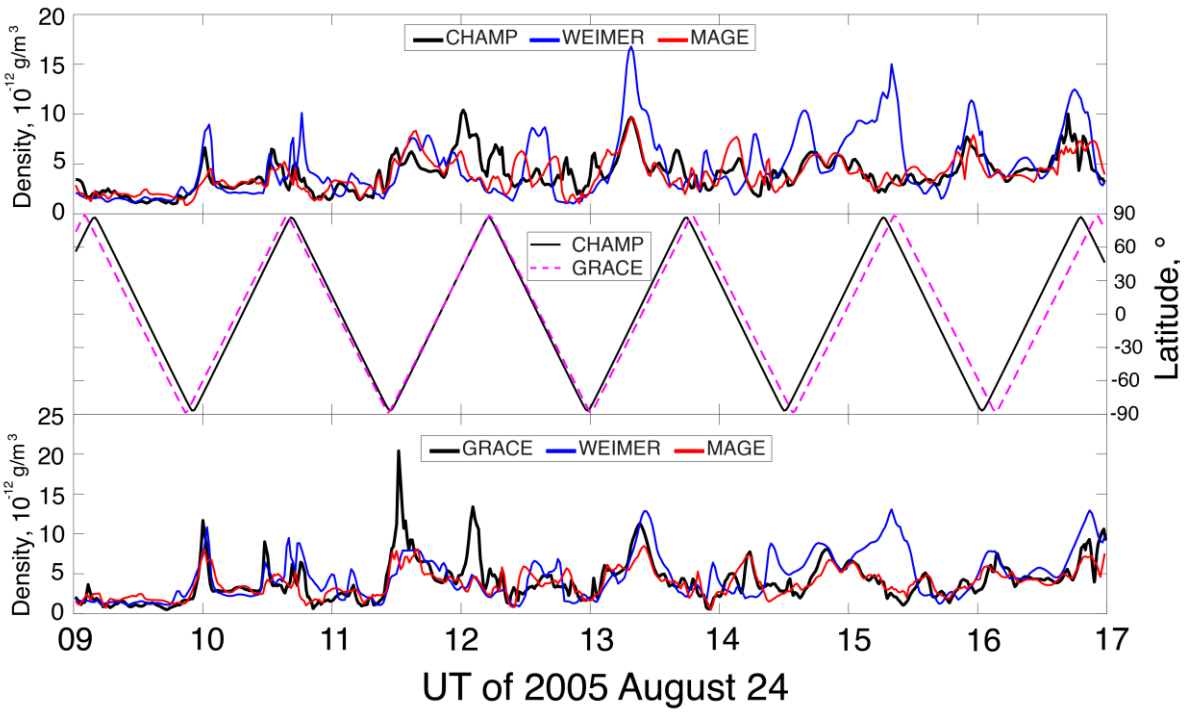

Figure 4: Modeled neutral density along the CHAMP (top) and GRACE (bottom) orbit from the WEIMER (blue) and MAGE (red) simulations. The orbital latitude (middle) for CHAMP (solid) and GRACE (dashed) are also shown.

latitudes for this geomagnetic storm. The larger and non-localized Joule heating from WEIMER (Figure 2) produces neutral density perturbations with incorrect propagation speeds and amplitudes, resulting in variability and perturbations at the lower latitudes to not be properly simulated. There are two large density peaks in GRACE data, one at 11:40 UT near the southern cusp and one at 12:05 UT near the northern cusp, are not captured by the MAGE.

An animation of the global neutral density distribution at 400km simulated by MAGE with virtual CHAMP and GRACE positions marked is shown in Movie S1 in the Supporting Information. While perturbations in the neutral density during quiet times occur, the perturbations are small in amplitude and agreement with the background neutral density dominates the root mean square error (RMSE) and coefficient of determine (R^2) calculation (Figure 5). During periods of more activity, plasma convection and auroral precipitation in the high-latitudes are significantly enhanced and greatly influence the neutral density. The heating also generates TADs that propagate away from the high-latitudes, and in some cases, reach the other hemisphere. When the TADs intersect with the CHAMP and GRACE trajectory, the satellites observe a local neutral density enhancement. While the WEIMER simulation captures and most of the time overestimates a few of the larger TADs observed by CHAMP and GRACE, MAGE captures significantly more TADs, especially the smaller amplitude ones. Since these observed density enhancements are the intersection of a propagating TAD and a moving spacecraft (CHAMP or GRACE), to simulate these density enhancements at that exact moment suggests that the TADs were both generated at the correct time and location, and also propagated with the correct speed to reach the spacecraft location at the right moment as observation. We note that both models are unable to capture the very large enhancements seen by GRACE during the storm main phase near 11:30 UT and 12:00 UT. Examination of Movie S1 show that these very large enhancements occur when GRACE is

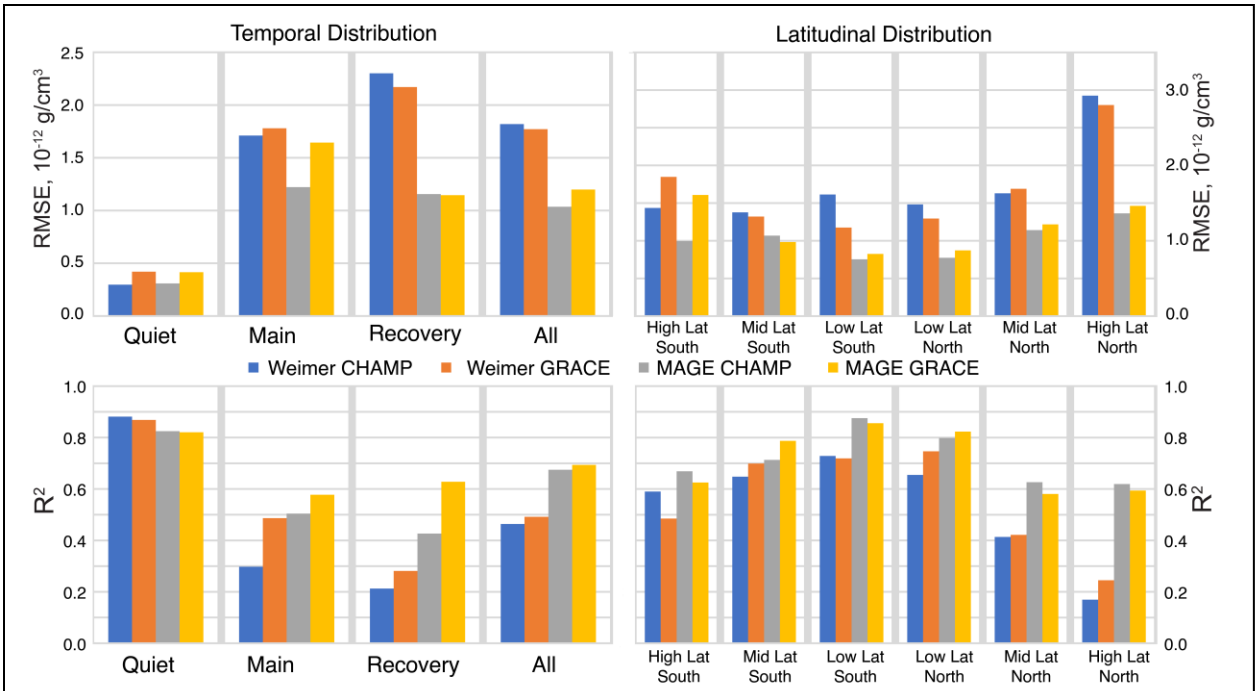

Figure 5: Temporal (left) and latitudinal (right) binning for the root mean square error (top) and coefficient of determination (bottom) between observed and simulated CHAMP and GRACE neutral density.

flying through the cusp region in the southern and northern hemispheres, respectively. Cusp soft precipitation (Zhang et al., 2012) and Alfvenic wave heating (Hogan et al., 2020) have not yet been implemented in the MAGE model which are likely the reason that the model misses these two outstanding density enhancements as thermospheric heating associated with these processes have been proposed to be an important process for local density perturbations (Zhang et al., 2012; Deng et al., 2013; Hogan et al., 2020).

The RMSE and R^2 between both models and the CHAMP and GRACE observations (Figure 5) quantify the overall model performance. The RMSE gives us a sense for how close the results are in value. While the R^2 value is a good measure of how the model captures the temporal morphology of the CHAMP and GRACE neutral densities, it does not necessarily account for any offsets or how close the model agrees with the actual measured value. Therefore, using RMSE and R^2 in combination provides a better sense of model performance than if either of them was used on its own. When the RMSE and R2 are binned based on geomagnetic activity throughout the day (Figure 5, left), we find that during quiet conditions the heating in the ionosphere-thermosphere is not as significant as during active times, so both models perform equally well there. During the main phase, the empirical specification from WEIMER is smoother and less dynamic than the physics-based MAGE model. This results in both a different total Joule power and a much smoother distribution without localized structures than MAGE. How this impacts model performance is reflected in significantly worse RMSE for WEIMER compared to MAGE for the main phase where WEIMER has 40% and 8% larger errors than MAGE for the CHAMP and GRACE tracks, respectively. In addition, R^2 shows that MAGE improves upon WEIMER in the ability to capture the morphology by 70% and 19%, respectively. While both model runs similarly lack the necessary heating in the cusp region, the whole geospace model of MAGE performs well

in capturing both the amplitudes, locations and timing of the observed density perturbations, indicating the necessity of using first principles whole geospace models such as MAGE to describe the storm-time behavior of the whole system and its temporal and spatial variability of different scales.

The recovery phase is vastly more complex than the main phase. The RMSE and R^2 for both WEIMER and MAGE are worse in the recovery phase than the main phase. With an inner magnetosphere model to provide a dynamic plasmasphere and ring current in the coupled MAGE model, the more realistic recovery phase produces a 100% better improvement across the board compared to WEIMER's RMSE and R^2. As seen in the RMSE and R^2 when the whole run ("All") is analyzed, the good performance during the quiet phase makes both model results appear to agree better with CHAMP and GRACE than they really are. However, it is still clear from analyzing "All" that MAGE is a significant improvement over statistical empirical specification of high latitude inputs using Weimer. Including a coupled model allows for the magnetosphere to impact the dynamic changes in the thermosphere-ionosphere and vice versa, for more self-consistent thermospheric heating, in the coupled MAGE reproduces well the morphology (as determined by R^2) and magnitude (as determined by RMSE) of the neutral density as observed by CHAMP and GRACE.

To better understand how differing high latitude dynamics impact the global thermosphere-ionosphere, we bin the CHAMP and GRACE comparisons into bins of 30° widths (Figure 5, right). Here, both the RMSE and R2 provide the same conclusion: MAGE performs significantly better in the high latitude northern hemisphere. Since only the high latitude are different between the models, the poorer performance in the mid and low latitudes by Weimer compared to MAGE is entirely due to the overestimated energy input by WEIMER (Figure 2) at the high latitudes propagating towards and impacting all other latitudes.

On a more local scale, we focus on two significant neutral density enhancements seen by CHAMP that occurs at 07:00 UT and 13:20 UT. The panels in Figure 6 show CHAMP clearly flying through TADs at these times. We note that GRACE had already flown through the TAD at 07:00 UT a few minutes prior and it would fly through the 13:20 UT TAD approximately 10 minutes later. Figure 6c shows the MAGE simulated difference in neutral density every minute along 12:00 LT, which is close to the CHAMP trajectory. This clearly highlights the neutral density perturbations associated with the TADs. By backtracking the perturbations occurring at 07:00 UT and 13:20 UT in Figure 6c, we find that the first neutral density enhancement at 07:00 UT was measured shortly after the TAD was generated near -60° LAT around 0645 UT in the southern hemisphere.

On the other hand, the second neutral density enhancement at 13:20 UT was generated much earlier near 09:30 UT at the northern high-latitudes. Snapshots from Movie S2 are shown in Figure 7 show a neutral density crest at the high-latitudes in the northern hemisphere that propagates to lower latitudes for many hours. By the time the crest has reached the equator and into the southern hemisphere where it is observed by CHAMP at 13:20 UT, the neutral density perturbation has significantly increased in amplitude after it intersected with a norward propagate TAD from the southern hemisphere. Many of other large lower latitude enhancements such as enhancement at CHAMP at 13:20 UT are also from TADs generated in either high-latitudes and have increased in amplitude by intersecting with other TADs as it propagates to lower latitudes, to produce a significantly larger perturbation away from the high-latitude TAD source regions.

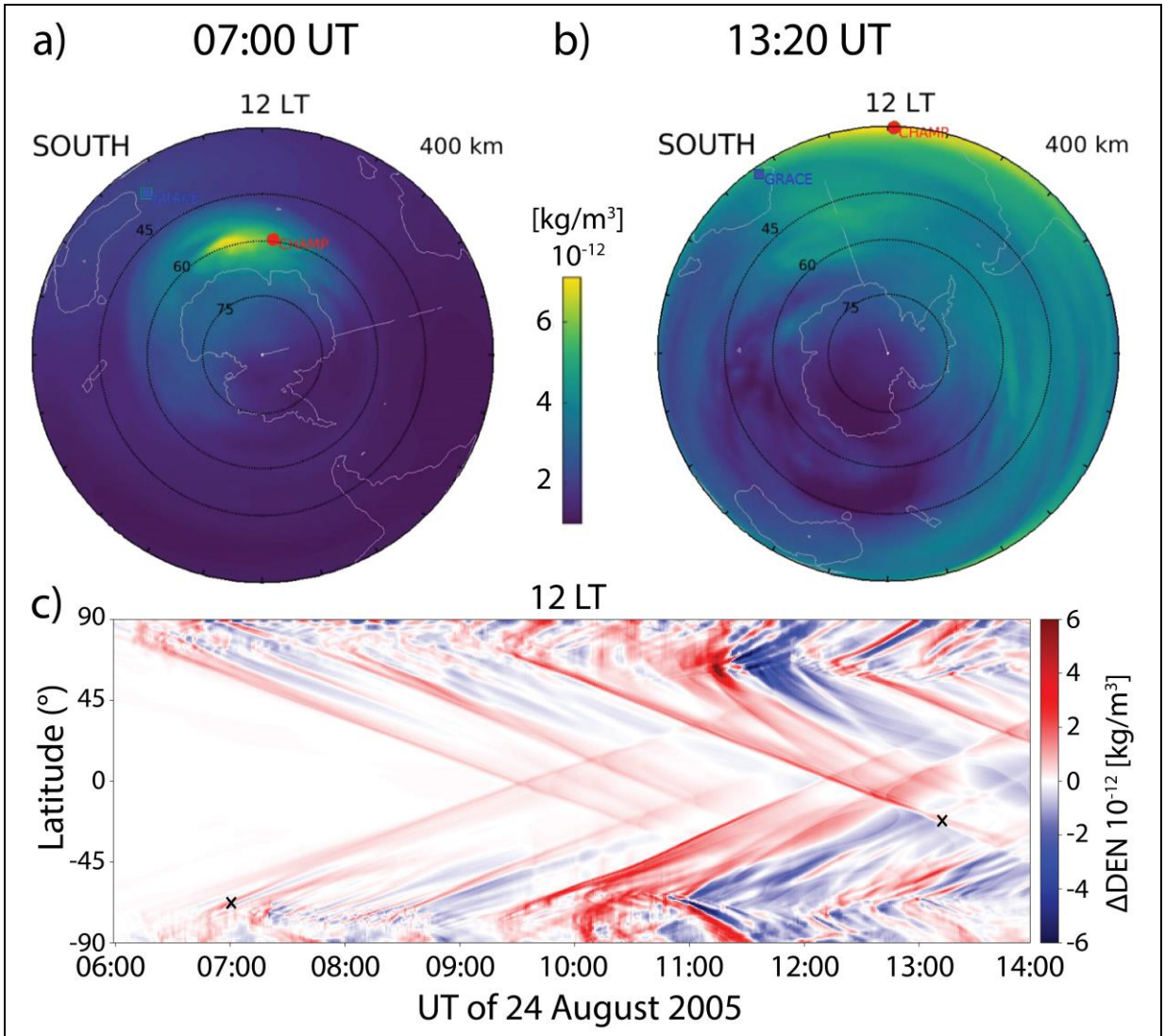

Figure 6: Snapshots from the animation Movie S1 with CHAMP (red) and GRACE (blue) positions marked. These two times correspond to when CHAMP observes a neutral density enhancement that are TADs (a) generated in the high-latitude and (b) when it has propagated to the lower latitude. (c) Minute difference of neutral density at 12LT between 0600UT and 1400UT showing clear TAD propagation with CHAMP latitude corresponding to (a) and (b) indicated with a black cross.

Due to the many small and medium scale TADs at the higher latitudes, it is difficult to track the large-scale TADs to the exact moment they were generated but following the propagation in both the Movie S1 and Movie S2, we estimate the generation of the 07:00 UT and 13:20 UT enhancements occurred at 06:45 UT and 09:30 UT, respectively. The height-integrated JH at both 06:45 UT and 09:30 UT were previously shown in Figure 2. The height-integrated JH at 06:45 for both MAGE and WEIMER are distributed in approximately the same latitudinal and longitudinal regions. Both show an enhanced JH region near 15 LT. However, because 06:45 is near the start of the main phase, heating from WEIMER ramps up more slowly, but it is much faster in the coupled MAGE, leading to more heating in the MAGE run. This produces a TAD with larger amplitude than that found in WEIMER, and more closely matches with GRACE and

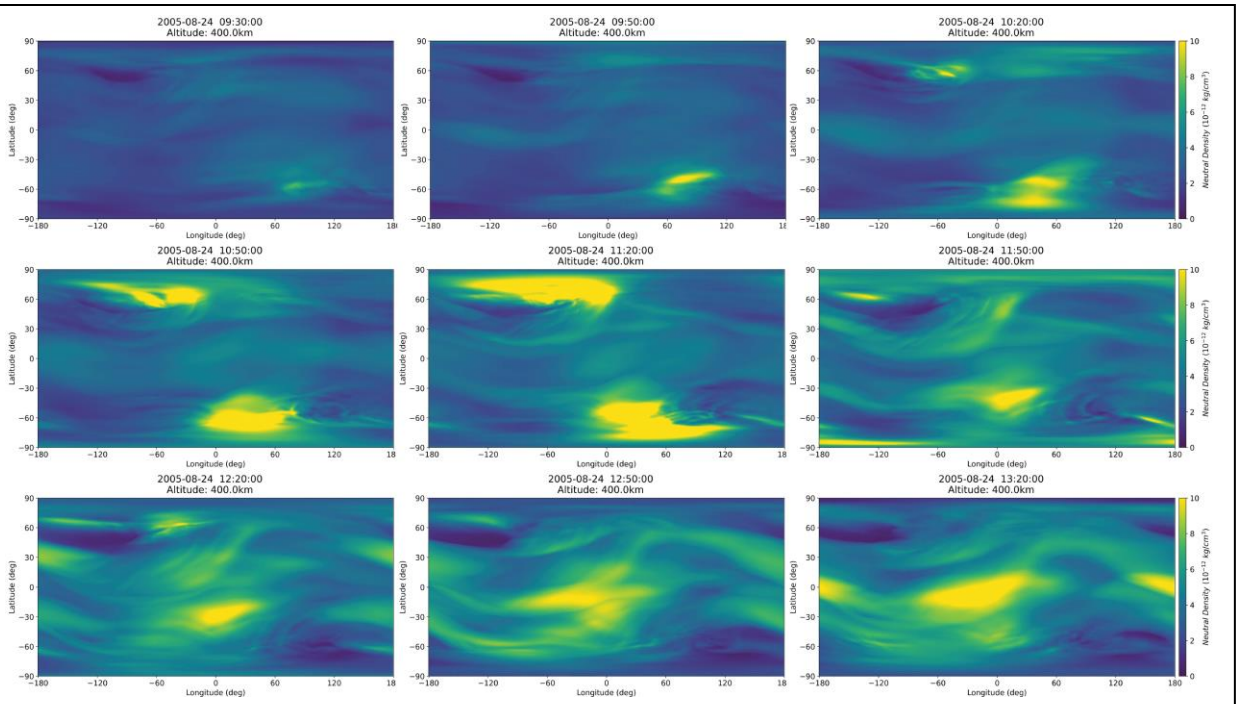

Figure 7: Snapshots from the animation Movie S2 that follows the neutral density perturbation observed by CHAMP at the lower latitude at 1320 UT.

CHAMP data. However, either the spatial timing or temporal timing of the TAD generated by MAGE is slightly misaligned, producing an underestimation of the GRACE and an overestimation of the CHAMP observations. For the height-integrated JH at 09:30 UT, the MAGE and WEIMER distributions are drastically different. The heating in WEIMER is distribution very broadly over a very large range of longitudes while the heating in MAGE is significantly more localized. This leads to WEIMER severely overestimating the enhancement in both the TAD source region at 09:30 UT and at low latitudes at 13:20 UT as compared to the observed density perturbations by CHAMP. While WEIMER appears to capture the amplitude of the perturbation at 13:20 UT from GRACE better than MAGE, this is mostly likely purely coincidence. Indeed, subsequent orbits of GRACE in WEIMER near the same region intersects large perturbations that are not seen in observations and is grossly overestimated along the CHAMP track. This implies that the broad WEIMER distribution of JH coincidentally produces a perturbation that matches with observation at 13:23 UT along GRACE. Capturing all of these correctly is necessary as is done most of the time by MAGE.

The global characteristic of neutral density perturbations is then dependent on not only the magnitude of the high latitude heating but also where the heating occurs, when the heating occurs, and the propagation speed and amplitude of the resulting high latitude disturbance. To further validate the accuracy of the MAGE Joule heating distribution, we compare the horizontal velocity measured by DMSP to those simulated by MAGE (Figure 8). The southern hemisphere passes (F14 and F16) have room for improvement. From Figure 6c, at around 09:30 UT in the southern hemisphere, there are multiple TADs being generated around this time that reach the northern hemisphere at around 12:00 UT. However, both models miss the neutral density perturbation in Figure 4 at 12:00 UT. The perturbations are likely from the southern hemisphere heating at 09:30

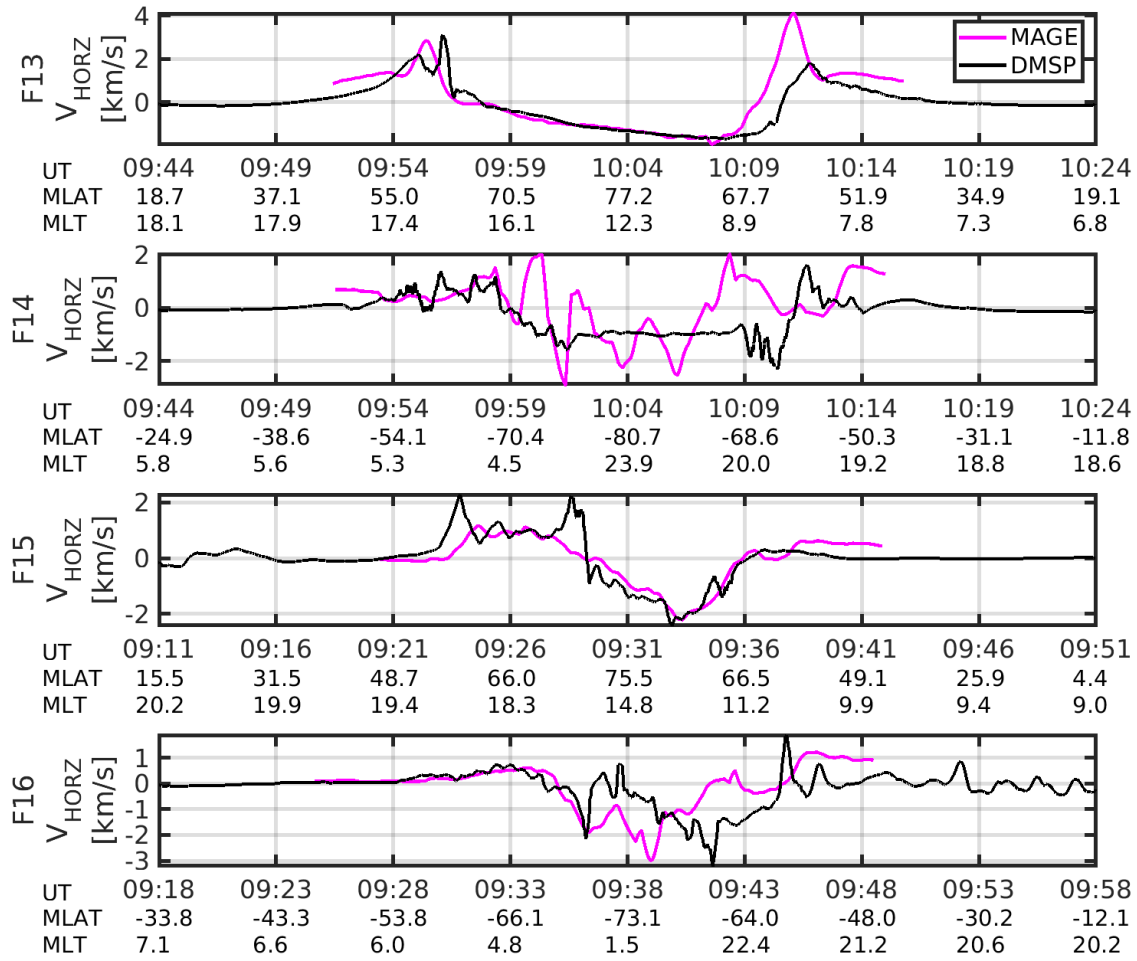

Figure 8: Horizontal velocity measured by DMSP F13, F14, F15, and F16 during the pass closest to 0930-1000 UT when a large amplitude TAD was generated in the northern and southern.

UT. For the northern hemisphere, both passes (F13 and F15) show that MAGE horizontal velocities agree surprisingly well with the observed. Overall, the capability to capture the generation, and evolution of the propagation speed and amplitude of the TAD that results in the observed low-latitude 13:20 UT neutral density enhancement represents a significant advancement and necessitates the need to have a coupled whole geospace model.

4 Conclusions

The MAGE coupled geospace model with high spatial resolving power in each region of geospace was used to simulate a geomagnetically active day of 24 August 2005 in which multiple thermospheric mass density enhancements are observed by CHAMP and GRACE. A fully coupled whole geospace model of MAGE with dynamically evolving high-resolution magnetosphere model and a high-resolution thermosphere-ionosphere model represents a significant improvement over using an empirical specification of high-latitude inputs of convection and precipitation in simulating Joule heating and the I-T responses. By flying virtual CHAMP and GRACE satellites through the simulations and compare with data, model performance and improvement was contrasted and quantified.

Our principal results are as follows:

- The coupled MAGE model reproduces both the magnitude and morphology of the storm-time neutral density perturbations as measured by CHAMP and GRACE. The first principles MAGE calculation of high latitude energy input from the magnetosphere to the thermosphere and ionosphere performs significantly better than statistical empirical specification of this input, especially during the main phase and recovery phases.
- Accurate description of both the distribution and magnitude of the localized Joule heating at high-latitudes is critical to produce TADs with the correct properties to produce neutral density enhancements not only at high-latitudes, but also in middle and low-latitudes that match with CHAMP and GRACE observations
- Localized large neutral density enhancements in the mid to low-latitudes are oftentimes the results of the intersection of multiple TADs generated in the high-latitudes

The MAGE model accurately captures both when and where the generation of TADs occurs and also their propagation speeds and amplitudes, demonstrating that a high resolution, fully coupled whole geospace model such as MAGE that can adequately resolve localized thermospheric heating and the associated physics of MIT coupling, including dynamic changes in convection electric fields and precipitation, is key to simulate the storm-time neutral density perturbations that are fundamental to upper atmosphere dynamics and space weather application of satellite drag. This is further reflected in the significant improvement in the RMSE and R^2 of MAGE compared to the standalone TIEGCM driven by the WEIMER empirical specification. The neutral density enhancements that are underestimated or missed by MAGE in the high-latitudes are most likely related to the cusp-region heating sources that are not yet included in MAGE. These include other sources of precipitation, such as direct entry cusp precipitation and broadband electron precipitation (Zhang et al., 2015), and Alfven wave heating (Hogan et al., 2020), that will be implemented in the MAGE model in due course.

Acknowledgments, and Data Sources

CHAMP and GRACE data are archived at http://tinyurl.com/densitysets. IMF and Solar wind data were provided by J.H. King, N. Papatashvilli at AdnetSystems, NASA GSFC and CDAWeb (http://omniweb.gsfc.nasa.gov/). We acknowledge support by the National Center for Atmospheric Research (NCAR), a major facility sponsored by the National Science Foundation under Cooperative Agreement No. 1852977 and NCAR System for Integrated Modeling of the Atmosphere (SIMA) reinvestment fund. This work is supported by NASA LWS under grants 80NSSC21K0008, 80NSSC19K0071, 80NSSC19K0835, 80NSSC17K0013, 80NSSC19K0080, 80NSSC17K0679, and 80NSSC20K0356, DRIVE Science Center for Geospace Storms (CGS) under grant 80NSSC20K0601, and O2R grant 80NSSC19K0241. Computing resources were provided by NCAR's Computational and Information Systems Laboratory (CISL).

MAGE thermosphere-ionosphere results can be found at https://doi.org/10.5281/zenodo.5587725 . The REMIX results from MAGE can be found at https://doi.org/10.5281/zenodo.5590561 . Standalone TIEGCM results driven by Weimer can be found at https://doi.org/10.5281/zenodo.5590500 .

References

Billett, D. D., Perry, G. W., Clausen, L. B. N., Archer, W. E., McWilliams, K. A., Haaland, S., et al. (2021). The relationship between large scale thermospheric density enhancements and the spatial distribution of Poynting flux. Journal of Geophysical Research: Space Physics, 126, e2021JA029205. https://doi.org/10.1029/2021JA029205

Bruinsma, S. L., & Forbes, J. M. (2007). Global observation of traveling atmospheric disturbances (TADs) in the thermosphere. Geophysical Research Letters, 34, L14103. https://doi.org/10.1029/2007GL030243

Bruinsma, S. L., & Forbes, J. M. (2009). Properties of traveling atmospheric disturbances (TADs) inferred from CHAMP accelerometer observations. Advances in Space Research, 43(3), 369–376. https://doi.org/10.1016/j.asr.2008.10.031

Bruinsma, S. L., and J. M. Forbes (2009), Properties of traveling atmospheric disturbances (TADs) inferred from CHAMP accelerometer observations, Adv. Space Res., 23, 369–376, doi:10.1016/j.asr.2008.10.031.

Bruinsma, S. L., and J. M. Forbes (2010), Large-scale traveling atmospheric disturbances (LSTADs) in the thermosphere inferred from CHAMP, GRACE, and SETA accelerometer data, J. Atmos. Sol. Terr. Phys., 72, 1057–1066.

Bruntz, R., R. E. Lopez, S. K. Bhattarai, K. H. Pham, Y. Deng, Y. Huang, M. Wiltberger, and J. G. Lyon (2012b), Investigating the viscous interaction and its role in generating the ionospheric potential during the whole heliosphere interval, J. Atmos. Sol. Terr. Phys., 83, 70–78, doi:10.1016/j.jastp.2012.03.016.

Burns, A. G., Killeen, T. L., Deng, W., Carignan, G. R., and Roble, R. G. (1995), Geomagnetic storm effects in the low- to middle-latitude upper thermosphere, J. Geophys. Res., 100(A8), 14673– 14691, doi:10.1029/94JA03232.

Connor, H. K., Zesta, E., Fedrizzi, M., Shi, Y., Raeder, J., Codrescu, M. V., & Fuller-Rowell, T. J. (2016). Modeling the ionosphere-thermosphere response to a geomagnetic storm using physics-based magnetospheric energy input: OpenGGCM-CTIM results. Journal Space Weather Space Climate, 6(A25), 1–15. https://doi.org/10.1051/swsc/2016019

Dang, T., Lei, J., Wang, W., Burns, A., Zhang, B., & Zhang, S.-R. (2018). Suppression of the polar tongue of ionization during the 21 August 2017 solar eclipse. Geophysical Research Letters, 45, 2918– 2925. https://doi.org/10.1002/2018GL077328

Dang, T., Zhang, B., Lei, J., Wang, W., Burns, A., Liu, H-L., Pham, K., Sorathia, K. (2021). Azimuthal averaging-reconstruction filtering techniques for finite-difference general circulation models in spherical geometry. Geoscientific Model Development, 1-30. doi:10.5194/gmd-14-859-2021

Deng, Y., Fuller-Rowell, T. J., Ridley, A. J., Knipp, D., and Lopez, R. E. (2013), Theoretical study: Influence of different energy sources on the cusp neutral density enhancement, J. Geophys. Res. Space Physics, 118, 2340-2349, doi:10.1002/jgra.50197.

Fok, M.-C., Buzulukova, N. Y., Chen, S.-H., Glocer, A., Nagai, T., Valek, P., and Perez, J. D. (2014), The Comprehensive Inner Magnetosphere-Ionosphere Model, J. Geophys. Res. Space Physics, 119, 7522– 7540, doi:10.1002/2014JA020239.

Forbes, J. M., G. Lu, S. Bruinsma, S. Nerem, and X. Zhang (2005), Thermosphere density variations due to the 15–24 April 2002 solar events from CHAMP/STAR accelerometer measurements, J. Geophys. Res., 110, A12S27, doi:10.1029/2004JA010856.

Guo, D., Lei, J., Ridley, A., & Ren, D. (2019). Low-density cell of the thermosphere at high latitudes revisited. Journal of Geophysical Research: Space Physics, 124, 521– 533. https://doi.org/10.1029/2018JA025770

Heelis, R. A., J. K. Lowell, and R. W. Spiro (1982), A model of the high-latitude ionosphere convection pattern, J. Geophys. Res., 87, 6339–6345, doi:10.1029/JA087iA08p06339.

Hogan, B., Lotko, W., & Pham, K. (2020). Alfvénic thermospheric upwelling in a global geospace model. Journal of Geophysical Research: Space Physics, 125, e2020JA028059. https://doi.org/10.1029/2020JA028059

Honkonen, I., Rastätter, L., Grocott, A., Pulkkinen, A., Palmroth, M., Raeder, J., Ridley, A. J., and Wiltberger, M. (2013), On the performance of global magnetohydrodynamic models in the Earth's magnetosphere, Space Weather, 11, 313– 326, doi:10.1002/swe.20055.

Kelley, M. C., Knudsen, D. J., and Vickrey, J. F. (1991), Poynting flux measurements on a satellite: A diagnostic tool for space research, J. Geophys. Res., 96(A1), 201– 207, doi:10.1029/90JA01837.

Kihn, E. A., Redmon, R., Ridley, A. J., and Hairston, M. R. (2006), A statistical comparison of the AMIE derived and DMSP-SSIES observed high-latitude ionospheric electric field, J. Geophys. Res., 111, A08303, doi:10.1029/2005JA011310.

Krall, J., Huba, J. D., Denton, R. E., Crowley, G., & Wu, T.-W. (2014). The effect of the thermosphere on quiet time plasmasphere morphology. Journal of Geophysical Research: Space Physics, 119, 5032–5048. https://doi.org/10.1002/2014JA019850

Krauss, S., Temmer, M., & Vennerstrom, S. (2018). Multiple satellite analysis of the Earth's thermosphere and interplanetary magnetic field variations due to ICME/CIR events during 2003–2015. Journal of Geophysical Research: Space Physics, 123, 8884– 8894. https://doi.org/10.1029/2018JA025778

Krauss, S., Temmer, M., Veronig, A., Baur, O., & Lammer, H. (2015). Thermosphere and geomagnetic response to interplanetary coronal mass ejections observed by ACE and GRACE: Statistical results. Journal of Geophysical Research: Space Physics, 120, 8848–8860. https://doi.org/10.1002/2015JA021702

Lei, J., Thayer, J. P., Burns, A. G., Lu, G., and Deng, Y. (2010), Wind and temperature effects on thermosphere mass density response to the November 2004 geomagnetic storm, J. Geophys. Res., 115, A05303, doi:10.1029/2009JA014754.

Liu, H., Lühr, H., and Watanabe, S. (2007), Climatology of the equatorial thermospheric mass density anomaly, J. Geophys. Res., 112, A05305, doi:10.1029/2006JA012199.

Liu, R., Lühr, H., & Ma, S.-Y. (2010). Storm-time related mass density anomalies in the polar cap as observed by CHAMP. Annales de Geophysique, 28(1), 165–180. www.ann-geophys.net/28/165/2010/. https://doi.org/10.5194/angeo-28-165-2010

Lopez, R. E., S. K. Bhattarai, R. Bruntz, K. Pham, M. Wiltberger, J. Lyon, Y. Deng, and Y. Huang (2012), The role of dayside merging in generating the ionospheric potential during the whole heliospheric interval, J. Atmos. Sol. Terr. Phys., 83, 63–69, doi:10.1016/j.jastp.2012.03.001.

Lu, G., Richmond, A. D., Lühr, H., and Paxton, L. (2016), High-latitude energy input and its impact on the thermosphere, J. Geophys. Res. Space Physics, 121, 7108– 7124, doi:10.1002/2015JA022294.

Matsuo, T., and Richmond, A. D. (2008), Effects of high-latitude ionospheric electric field variability on global thermospheric Joule heating and mechanical energy transfer rate, J. Geophys. Res., 113, A07309, doi:10.1029/2007JA012993.

Mayr, H. G., I. Harris, F. A. Herrero, N. W. Spencer, F. Varosi, and W. D. Pesnell (1990), Thermospheric gravity waves: Observations and interpretation using the transfer function model (TFM), Space Sci. Rev., 54, 297–375.
Merkin, V. G., and Lyon, J. G. (2010), Effects of the low-latitude ionospheric boundary condition on the global magnetosphere, J. Geophys. Res., 115, A10202, doi:10.1029/2010JA015461.
Mukhopadhyay, A., Jia, X., Welling, D.T., Liemohn, M.W. (2021), Global Magnetohydrodynamic Simulations: Performance Quantification of Magnetopause Distances and Convection Potential Predictions, Front. Astron. Space Sci., 8:637197. doi: 10.3389/fspas.2021.637197.
Oliveira, D. M., & Zesta, E. (2019). Satellite orbital drag during magnetic storms. Space Weather, 17, 1510– 1533. https://doi.org/10.1029/2019SW002287
Prolss, G. (2011), Density perturbations in the upper atmosphere caused by the dissipation of solar wind energy, Surv. Geophys., 32, 101–195, doi:10.1007/s10712-010-9104-0.
Qian, L., Burns, A. G., Emery, B. A., Foster, B., Lu, G., Maute, A., ... & Wang, W. (2014). The NCAR TIE-GCM: A community model of the coupled thermosphere/ionosphere system. Modeling the ionosphere-thermosphere system, 201, 73-83.
Roble, R. G. & Ridley, E. C. (1987). An auroral model for the NCAR thermosphere general circulation model (TGCM), Annales Geophysicae, 5A (6), 369-382.
Richmond, A. D. (2010), On the ionospheric application of Poynting's theorem, J. Geophys. Res., 115, A10311, doi:10.1029/2010JA015768.
Richmond, A., Ridley, E. C., & Roble, R. G. (1992). A thermosphere/ionosphere general circulation model with coupled electrodynamics. Geophysical Research Letters, 19(6), 601–604. https://doi.org/10.1029/92GL00401
Sorathia, K. A., Merkin, V. G., Panov, E. V., Zhang, B., Lyon, J. G., & Garretson, J., et al. (2020). Ballooning-interchange instability in the near-Earth plasma sheet and auroral beads: Global magnetospheric modeling at the limit of the MHD approximation. Geophysical Research Letters, 47, e2020GL088227. https://doi.org/10.1029/2020GL088227
Sutton, E. K. (2011), Accelerometer-derived atmospheric densities from the CHAMP and GRACE accelerometers: Version 2.3, Tech. Memo, Air Force Res. Lab., Kirtland Air Force Base.
Toffoletto, F. R., S. Sazykin, R. W. Spiro, and R. A. Wolf (2003). Inner magnetosphere model-ing with the Rice Convection Model, Space Sci Rev, 107, 175–196.
Vanhamäki, H., Yoshikawa, A., Amm, O., and Fujii, R. (2012), Ionospheric Joule heating and Poynting flux in quasi-static approximation, J. Geophys. Res., 117, A08327, doi:10.1029/2012JA017841.
Wang, W., M. Wiltberger, A. G. Burns, S. Solomon, T. L. Killeen, N. Maruyama, and J. Lyon (2004), Initial results from the CISM coupled magnetosphere-ionosphere-thermosphere (CMIT) model: Thermosphere ionosphere responses, J. Atmos. Sol. Terr. Phys., 66, 1425–1441.
Wang, W., Talaat, E. R., Burns, A. G., Emery, B., Hsieh, S., Lei, J., and Xu, J. (2012), Thermosphere and ionosphere response to subauroral polarization streams (SAPS): Model simulations, J. Geophys. Res., 117, A07301, doi:10.1029/2012JA017656.
Weimer, D. R. (2005), Improved ionospheric electrodynamic models and application to calculating Joule heating rates, J. Geophys. Res., 110, A05306, doi:10.1029/2004JA010884.

Wiltberger, M., Rigler, E., Merkin, V., & Lyon, J. (2017). Structure of high-latitude currents in magnetosphere-ionosphere models. Space Science Reviews, 206, 575–598. https://doi.org/10.1007/s11214-016-0271-2

Wiltberger, M., Rigler, E., Merkin, V., & Lyon, J. (2017). Structure of high-latitude currents in magnetosphere-ionosphere models. Space Science Reviews, 206, 575–598. https://doi.org/10.1007/s11214-016-0271-2

Xu, L. et al. (2008), A 2-D comparison of ionospheric convection derived from SuperDARN and DMSP measurements, Adv. Space Res., 42, 1259–1266.

Zhang, B., Lotko, W., Brambles, O., Wiltberger, M., Wang, W., Schmitt, P., and Lyon, J. (2012), Enhancement of thermospheric mass density by soft electron precipitation, Geophys. Res. Lett., 39, L20102, doi:10.1029/2012GL053519.

Zhang, B., Lotko, W., Brambles, O., Wiltberger, M., & Lyon, J. (2015). Electron precipitation models in global magnetosphere simulations. Journal of Geophysical Research: Space Physics, 120, 1035–1056. https://doi.org/10.1002/2014JA020615

Zhang, B., Sorathia, K. A., Lyon, J. G., Merkin, V. G., Garretson, J. S., & Wiltberger, M. (2019a). GAMERA: A three-dimensional finite-volume MHD solver for non-orthogonal curvilinear geometries. The Astrophysical Journal Supplement Series, 244(1), 20. https://doi.org/10.3847/1538-4365/ab3a4c

Zhang B., Sorathia, K. A., Lyon, J. G., Merkin, V. G., & Wiltberger, M. (2019b). Conservative averaging-reconstruction techniques (Ring Average) for 3-D finite-volume MHD solvers with axis singularity. Journal of Computational Physics, 376, 276-294, https://doi.org/10.1016/j.jcp.2018.08.020.